ANNALI DI GEOFISICA, VOL. XXXIX, N. 1, January 1996

Geoelectrical study of archaeological structures in the Himera plane (North-western Sicily)

Pietro Cosentino ([1]), **Dario Luzio** ([1]) **and Edoardo Rotigliano** ([2])
([1]) *Istituto di Geofisica Mineraria, Università di Palermo, Italy*
([2]) *Geotop, Palermo, Italy*

Abstract
This paper presents the results obtained from a geoelectrical study carried out on the Himera plane for archaeological research. Both the tripotential method and the dipole-dipole profile method have been used on a 40 m × 40 m investigation area in order to obtain several resistivity maps. The latter show different geoelectrical anomalies, the shape of which allows us to interpret simple archaeological structures, consistent with current knowledge of ancient Himera sites. Furthermore, the study of the whole set of data in the resistivity domain has allowed us to infer some other characteristics from the subsequent geological process of alluvial covering of the site.

Key words *geoelectrical prospecting – tripotential method – pseudo-section – archaeology*

1. Introduction

A geoelectrical integrated survey, similar to that previously carried out in the Archeological Park of Selinunte (Cosentino *et al.*, 1992), was performed in the archaeological area of Himera.

This archaeological area is located on the northern coast of Sicily, about thirty kilometers from Palermo. The ancient Himera village was founded in 648 b.C. by Ionians and Dorians and was destroyed two hundred and forty years later. The ancient village extended from the western part of the plane along the mouth of the Himera river up to the two south-neighboring hills. At present only the upper part of the ancient village has been excavated, while the lower part is still fully covered by cultivated fields, the only outcrop available being the basement of the Vittoria Temple. According to archaeological studies this area is supposed to be rich in buried archaeological structures. The purpose of the geoelectrical survey was to detect these archaeological structures by discriminating geophysical anomalies.

2. Field measurement and data processing

An area of 40 m × 40 m was covered with a regular grid of copper electrodes with square mesh having 2 m spacing to carry out tripotential and dipole-dipole measurements. The area chosen (fig. 1) is characterized by a flat morphology and by a regular thin overburden mainly composed of alluvial clays. These two characteristics of the site produced sets of data poorly affected by noise due to topographic and geolithological anomalies. Some archaeological studies seem to indicate the presence in the area of roads linking the ancient village to the sea, orthogonally-bound with respect to the coastline; consequently, in order not to bias the measurements in the direction of presumed road location, we tried to rotate the main axes of the grid with respect to that direction. Unfortunately the size and the shape of the area available for

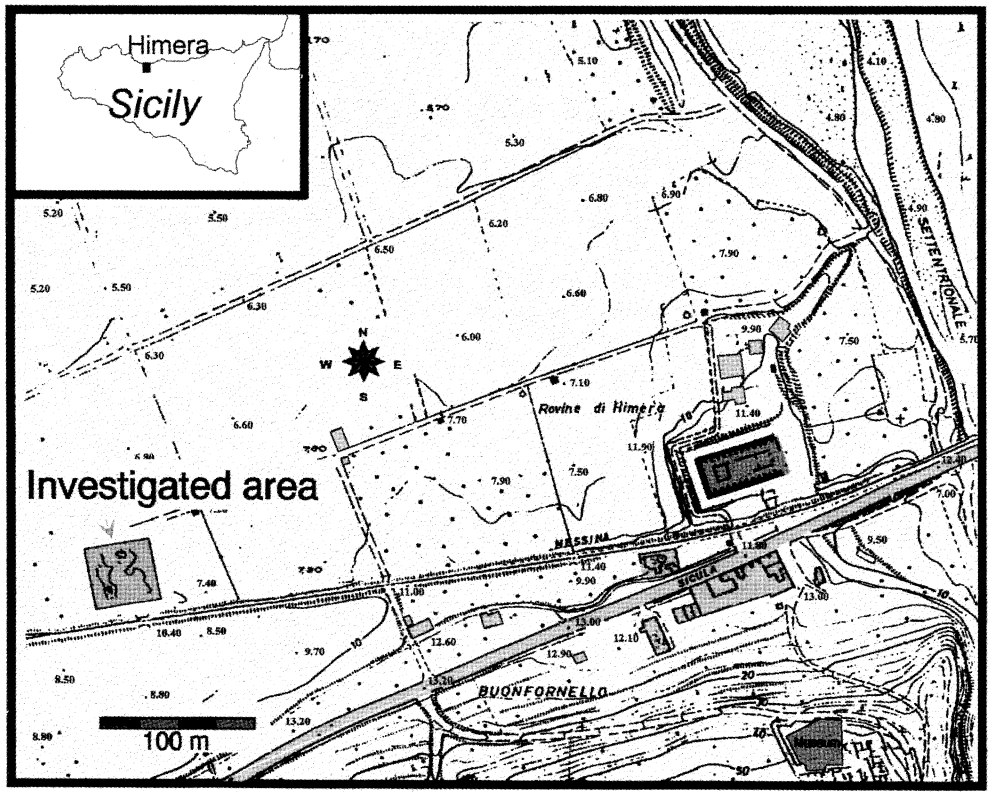

Fig. 1. Map of a part of the Buonfornello plane, at the western part of the mouth of the Northern Imera river. In the eastern part of the map the basement of the Vittoria temple is shown. The declivity of the hill of the ancient high Himera village can be observed at the bottom of the map.

the investigation as well as the presence of a railway embankment allowed only a minor rotation of a few degrees (the X axis was fixed at about 78°, while Y was about 348°).

441 copper electrodes were located as carefully as possible in the measurement grid in order to reduce the possible errors in the geometric distances between adjacent electrodes. The maximum residual errors in the edges of the meshes were estimated within 3 cm, corresponding to about 1.5%.

The data were acquired using a resistivity meter with an accuracy of 0.01 mV and 0.01 mA in the standard stacking cycle. The number of repetitions in each measurement cycle was set to obtain a safety level of reliability in the measures. Several measurement tests carried out for randomly selected measure-samples showed that the maximum relative measure-error was at 1.2% level. The data acquisition process was carried out without any particular problem due to signal-to-noise ratios or weather conditions.

The tripotential measures were acquired using three different spacing values between adjacent electrodes (spacing equal to 2, 4 and 6 m, hereafter respectively S2, S4 and S6) in order to investigate three different thickness of the overburden. The dipole-dipole profiles were executed using dipole amplitudes of 2 m, and dipole order ranging from the second to

the fifth one to progressively increase the depth of investigation.

These measurement methods were carried out using both the orthogonal main directions of the grid. Therefore the investigation project involved the acquisition of 1890 measures for α-resistivity, as many for β-resistivity and for γ-resistivity measures, and 2772 dipole-dipole measures. The whole set of data was acquired in about 85 h, using a multipolar cable and a roll along switch (24 channels).

For each of the three subsets of tripotential data acquired with different spacing (namely S2, S4 and S6) the tripotential errors ε_i (Habberjam, 1979) were evaluated using the following normalization:

$$\varepsilon\ (\%) = 300 \times (R_\alpha - R_\beta - R_\gamma) \,/\, (R_\alpha + R_\beta + R_\gamma). \tag{2.1}$$

The histograms showing the frequency distribution of the three subsets of data are presented in fig. 2. The distributions are generally irregular, the mean being negative and its absolute values growing for S4 and S6 subsets. The maximum absolute value of skewness is presented by the S4 set. These distributions show that the errors are mainly due to the contact resistance of the electrodes as well as to the resistivity model of the investigated volumes (Colletti *et al.*, 1995) which progressively increase in depth from S2 to S6.

The composed resistivity ρ_μ and ρ_τ were finally calculated by the tripotential resistivity ρ_α, ρ_β and ρ_γ, once corrected according to the minimum-distance method (Cosentino and Luzio, 1994):

$$\rho_\mu = \sqrt{3} \cdot (\rho_\alpha + \rho_\beta + \rho_\gamma)/3, \tag{2.2}$$

$$\rho_\tau = \sqrt{42} \cdot (\rho_\alpha - 5\,\rho_\beta + 4\,\rho_\gamma)/14. \tag{2.3}$$

The dipole-dipole data were arranged to construct the conventional pseudo-sections (Hallof, 1957), which in turn were processed using the Fraser filters (Fraser, 1981). These were slightly modified by assigning different weights to the different levels of the filter-window in order to emphasize or depress the influence of the various depths of the investigated volumes.

3. Analysis of data in the space domain

Using the whole set of the tripotential data many resistivity maps were obtained. In fact the set was divided into three different subsets, namely ρ_α, ρ_β and ρ_γ. For each of them, the two sets of measured values – *i.e.* those measured along the X and Y axes – were used to construct the resistivity maps. So, the S2 α, β and γ-resistivities, with a spacing of 2 m, are presented in fig. 3. It shows the X maps, the Y

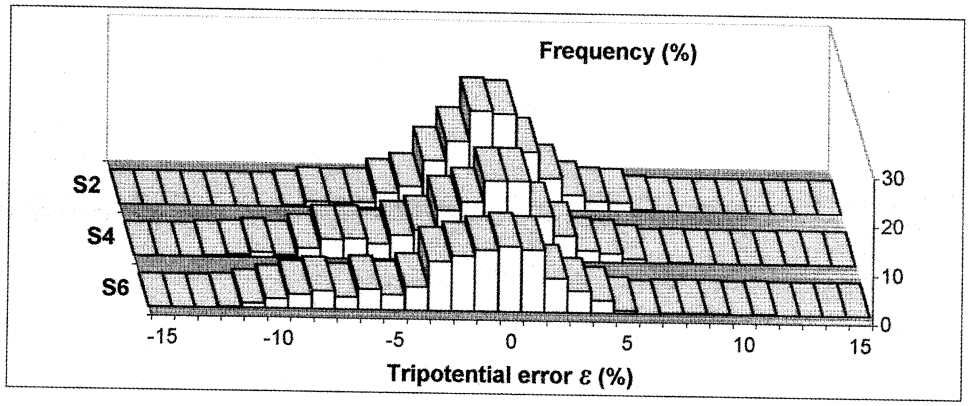

Fig. 2. Distribution of the ε_i for the three subsets of tripotential data.

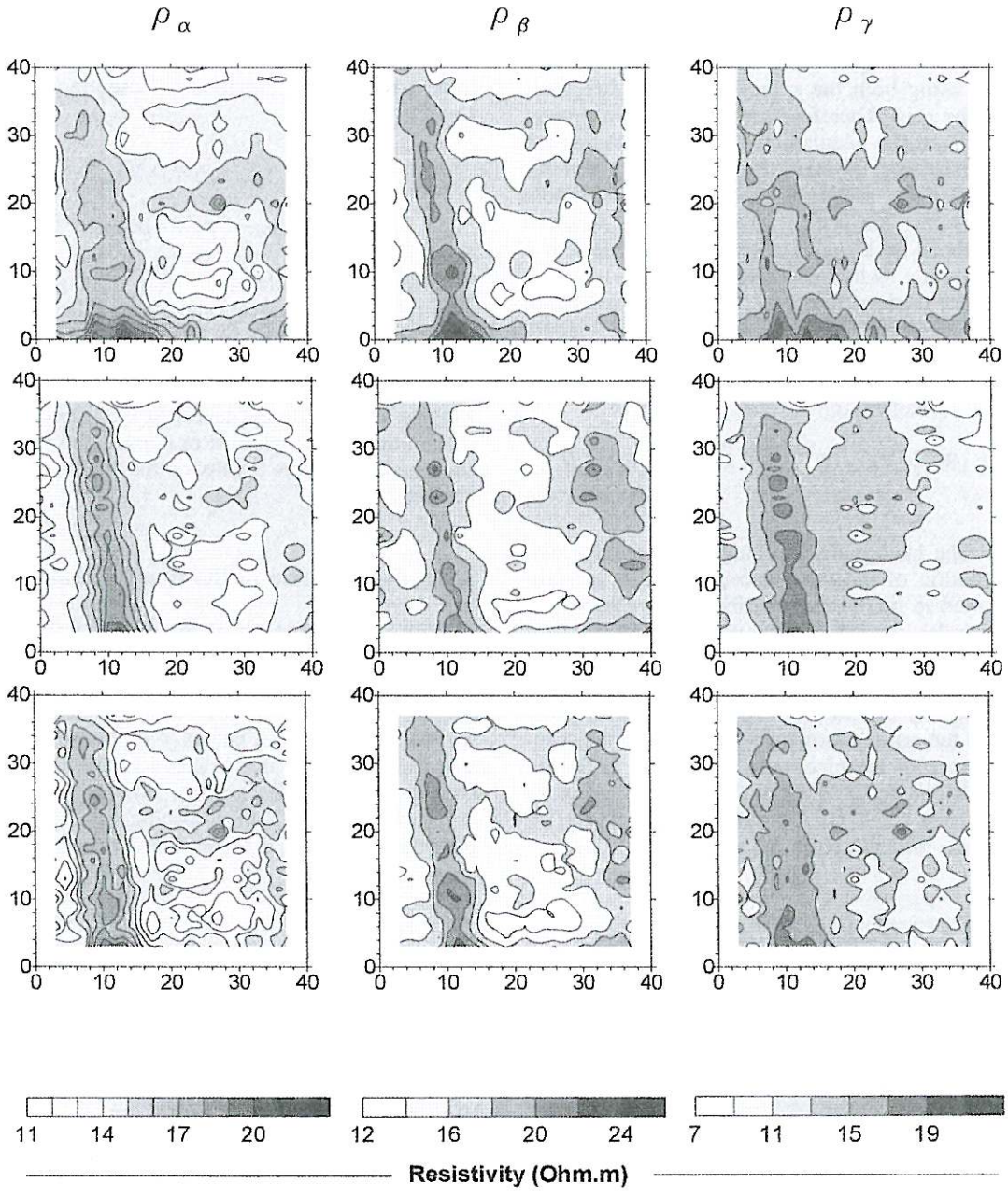

Fig. 3. Maps of space behavior of ρ_α, ρ_β and ρ_γ of the S2 set of data. From the top to the bottom the rows refer to *X*, *Y* and «integrated» data.

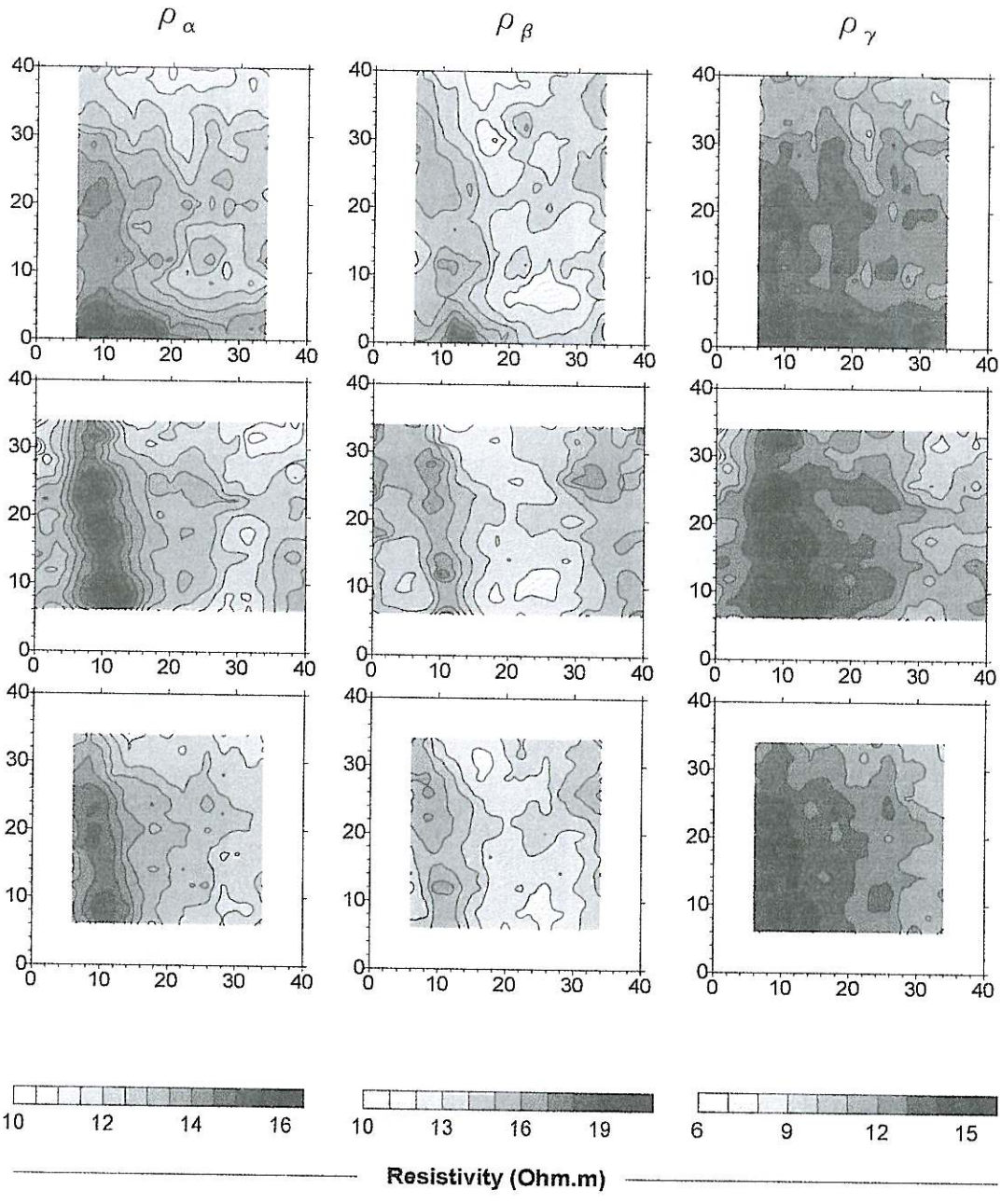

Fig. 4. Maps of space behavior of ρ_α ρ_β and ρ_γ of the S4 set of data. From the top to the bottom the rows refer to *X*, *Y* and «integrated» data.

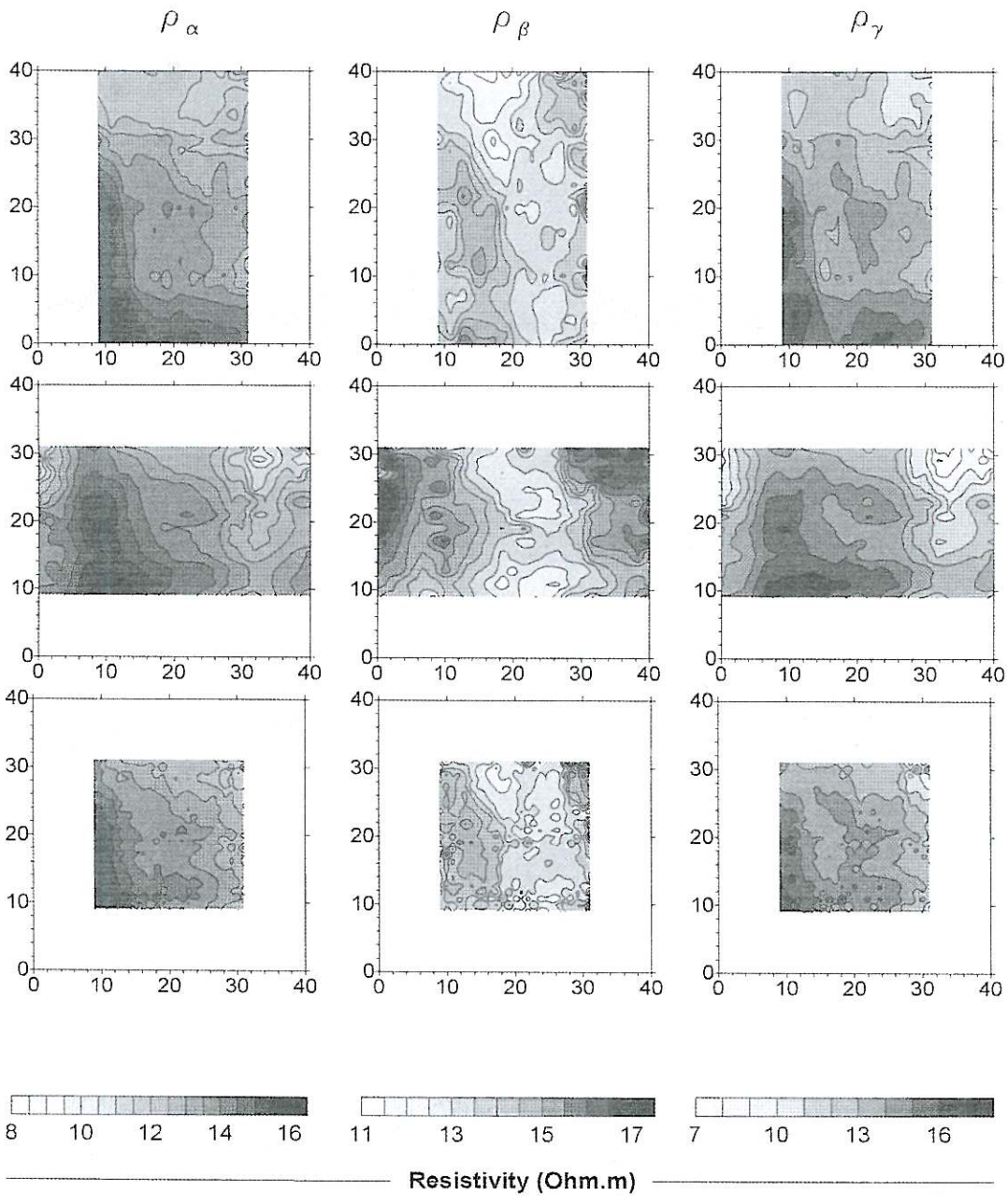

Fig. 5. Maps of space behavior of ρ_α, ρ_β and ρ_γ of the S6 set of data. From the top to the bottom the rows refer to X, Y and «integrated» data.

maps and the «integrated» ones, *i.e.* those obtained by the integration of the two sets of data. A large resistive straight anomaly is immediately evident; it is located along the axis going from the point $X = 11$, $Y = 4$ (hereafter [11, 4]) to the point [7, 37], being about 6 m in breadth. It is better evident in the X maps for α and γ-resistivities, while for the β-resistivities the Y map seems to be the clearest one. Furthermore the maps seem to indicate the presence of two conductive anomalies: the larger one is characterized by a roughly quadrangular shape, the vertices being located in the points [17, 4], [34, 4], [33, 18] and [16, 18], the minor one is less regular and it is located (see the Y β-resistivity map) between the points [13, 30] and [28, 30]. All the S2 maps present the field of minor low-wavelength anomalies.

The same kind of maps, obtained using the data acquired with a spacing of 4 m and 6 m (that is, S4 and S6), are presented, respectively, in figs. 4 and 5. The lateral blind areas in the X and Y maps, as well as their increase for larger values of the electrode spacings, are due to the mentioned acquisition scheme. The cumulated effects are obviously evident in the decreasing extents of the integrated maps.

Much of the S4 maps still show the main resistive anomaly, while some of them, especially the integrated γ-resistivity map, seem very irregular, without any particular recognizable pattern.

The main resistive anomaly in the S6 maps was also generally detected, even if its shape is lightly deranged and smoothed. It should be noticed that in the β-resistivity X map the axis of this anomaly appears to be displaced at about 4 m along the X direction.

Six maps were obtained, three for μ-resistivity and three for τ-resistivity, referring to S2, S4 and S6 data. The τ-resistivity maps seem to be very disturbed, as the low wavelength anomalies with no noticeable geometrical shapes show; so, the only maps here presented are the μ-resistivity maps, arranged in a unified perspective view (fig. 6) including S2, S4 and S6 maps in a layered diagram according to the depth of investigation of every map. These maps show the main characteristics of the electric anomalies, the predominant resistive one and the minor ones, both resistive and conductive, which very probably delineate a small part of the layout of the Himera ancient village. The same picture evidences the progressive disappearance of the anomalies according to the increase in the spacing, so that a depth between 1 and 2 m can be assigned to the archaeological layer in the investigated area.

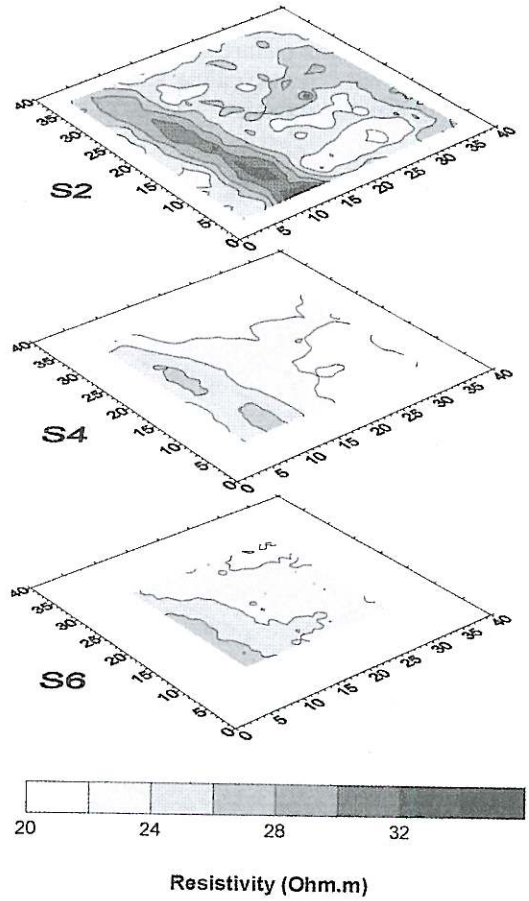

Fig. 6. 3-D view of the ρ_μ maps for different depths of investigation. The resistivity values in the gray-tone scale are expressed in Ohm.m.

Concordant information is given by the multiplanar perspective view presented in fig. 7, which was obtained using the integrated dipole-dipole data pertaining to different orders

of receiver dipole, therefore to different investigation depths. This picture also evidences the resistive bedrock, corresponding to a shore terrace of calcarenite deposits.

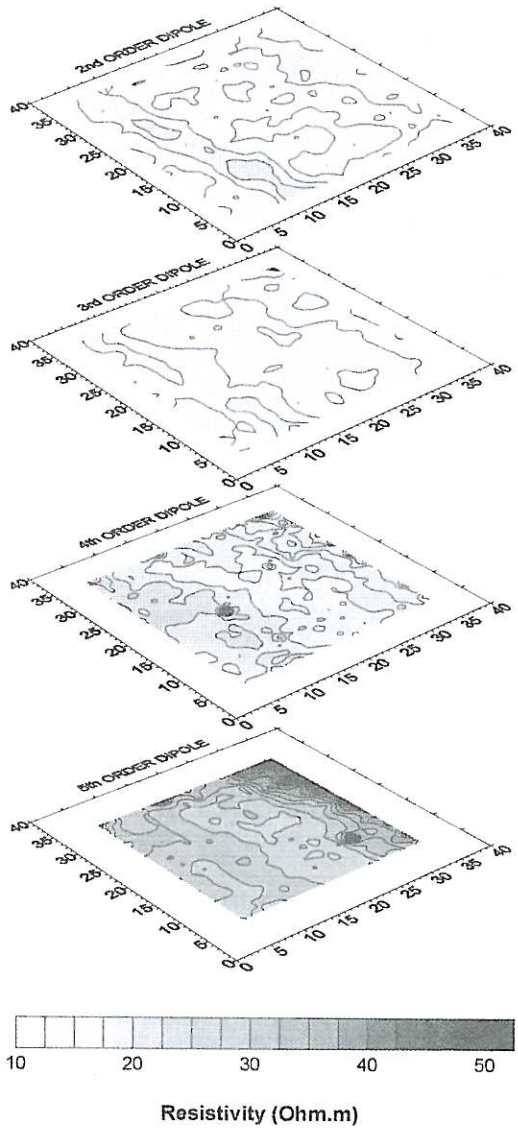

Fig. 7. 3-D view of the dipole-dipole resistivity maps for different depths of investigation. The resistivity values in the gray-tone scale are expressed in Ohm.m.

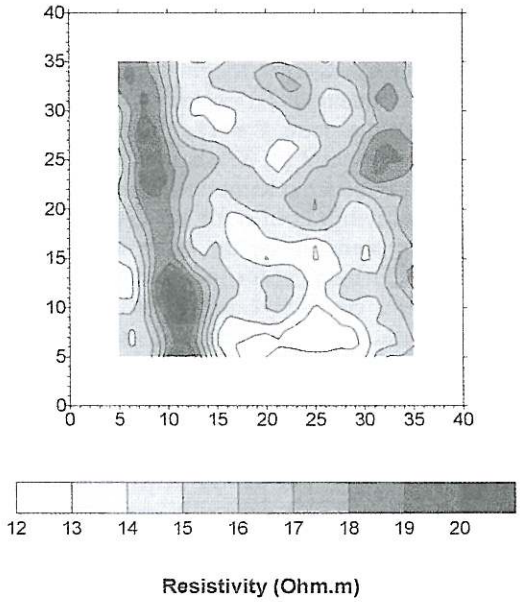

Fig. 8. Map of the dipole-dipole resistivity filtered (after Fraser) only using the pseudosection data from 1st and 2nd levels. The resistivity values in the gray-tone scale are expressed in Ohm.m.

Finally fig. 8 presents a picture obtained by a superimposition of the Fraser filter on the data acquired using the 2nd and 3rd order dipoles in both X and Y directions. This picture seems to be highly representative of the geometric shapes in the archaeological layer: the analysis of the shapes of the contour lines seems to suggest the presence of two other axes of resistive anomalies. The first axis is roughly parallel to the mentioned main axis of resistive anomaly, even if it is only partially but clearly observable along the segment joining the points [32, 35] and [37, 5]; the other axis, which is not so distinct, is roughly orthogonal to the first one and is placed between the points [32, 25] and [9, 22].

Perhaps, the interpretation of these anomalies in terms of archaeological structures is simple enough: in fact the shape, the directions and the widths of these resistive anomaly axes and also their respective distances, seem to easily identify them as a part of a main road of

the ancient village and as minor connected lanes. In particular, the direction of the main roads is consistent with the assumed general direction of the global layout of the ancient village, *i.e.* the direction from the southern hills to the sea.

4. Analysis of tripotential data in the resistivity domain

In order to identify some general characteristics of the possible interpretative models it may be useful to consider the S2, S4 and S6 subsets of tripotential data in the resistivity domain. This analysis is generally carried out using the ρ_τ-ρ_μ diagrams (Cosentino and Luzio, 1994).

As the three subsets of the tripotential data give a highly scattered cloudy pattern (table I), probably due to large and minor heterogeneities, as well as to the residual errors on every apparent resistivity, the subsets were filtered in order to identify any general trends. So, the classical moving average technique along the ρ_μ axis was applied to every subset of data, using 1 Ohm.m as width of the averaging box as well as of the sampling step.

The diagrams showing the behavior of the filtered data of the three subsets S2, S4 and S6 are presented in figs. 9, 10 and 11 respectively. The correlation among the values of the composed resistivities increases with the increase in investigation depth; this is consistent with the results obtained on a two-layer model characterized by variations in thickness of the first layer (Cosentino and Luzio, 1994; Cosentino *et al.*, 1996). A 3-layers model, namely Resistive-Conductive-Resistive with variable thicknesses of the first and second layers, can explain the progressive increase in ρ_τ when the depth of investigation grows.

It is useful to distinguish the various parts of the maps in order to discriminate each single homogeneous part of the map in the previous diagrams. In fact figs. 9, 10 and 11 present the data relative to the main road as well as those referring to the conductive area (probably a block). The latter data were filtered using the same procedure as for the data referring to the whole area investigated. The data pertaining to smaller and homogeneous areas obviously are much more correlated in both domains and the correlation coefficient grows when the depth of investigation increases. The positive values of ρ_τ in the S6 diagram for the main resistive area indicate that the deep resistive prevails compared to the shallow one, as the synthetic tests on two layers simple models have shown (Cosentino and Luzio, 1994). Also the data connected with conductive area show the same growing correlation when the depth of investigation increases, but the correlation coefficient already seems significant for the S4 data. This could indicate that the conductive layer is thinner. A conclusive hypothetical qualitative model of three different parts of the investigated area is presented in fig. 12.

Table I. Main statistical characteristics of the three subsets of ρ_τ-ρ_μ data

	Subset S2	Subset S4	Subset S6
Number of samples	756	630	504
Minimum ρ_τ value	−35.18	−27.79	−37.00
Maximum ρ_τ value	19.74	10.31	11.15
Mean ρ_τ value	−6.82	−2.82	−1.70
Standard deviation	7.39	5.68	6.51
ρ_τ-ρ_μ correlation coefficient	0.05	0.20	0.62

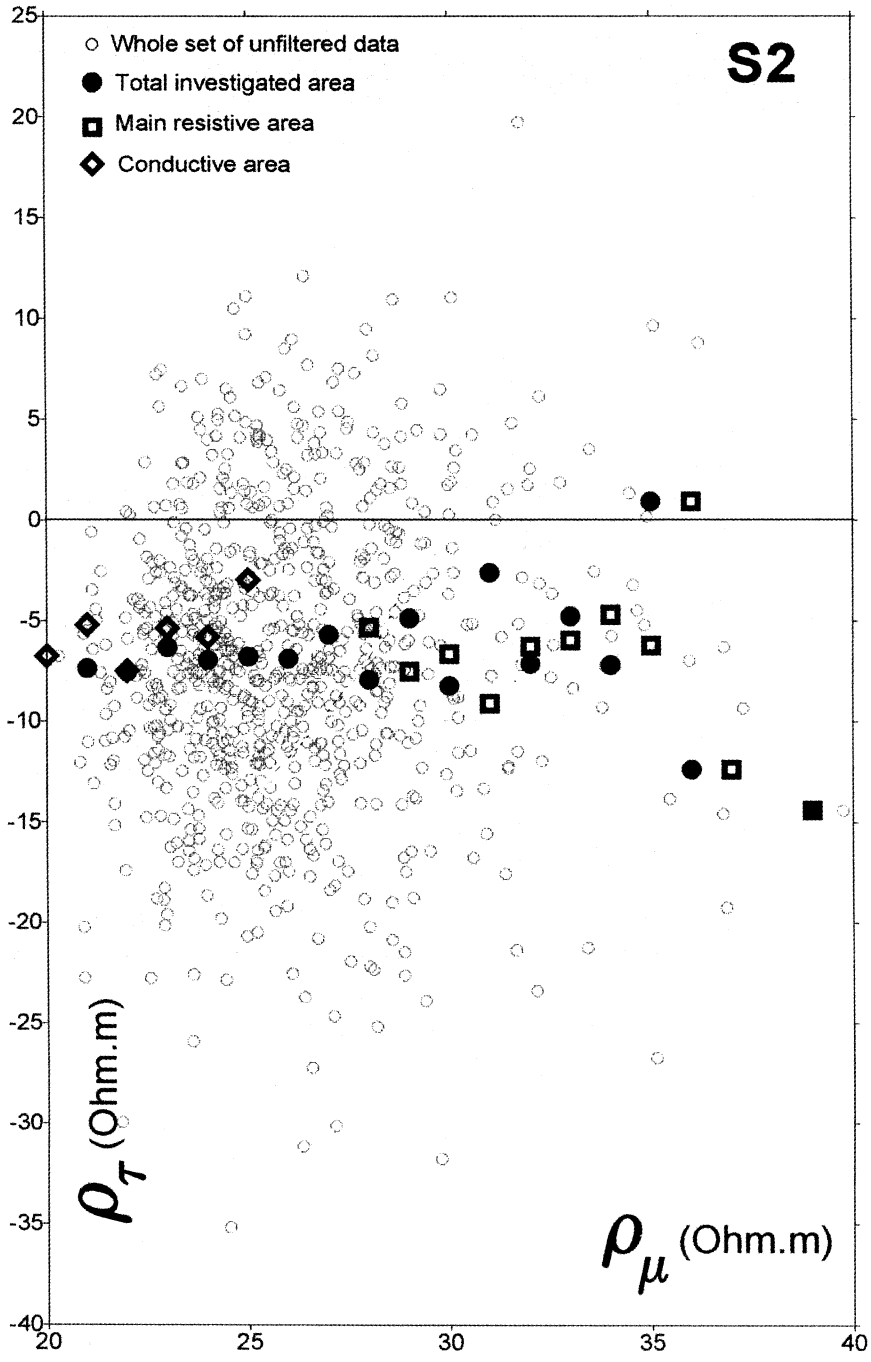

Fig. 9. Diagram of ρ_τ versus ρ_μ for S2 set of tripotential data. Filtered data (in bold) were obtained using moving average filtering with a box of 1 Ohm.m along the ρ_μ axis.

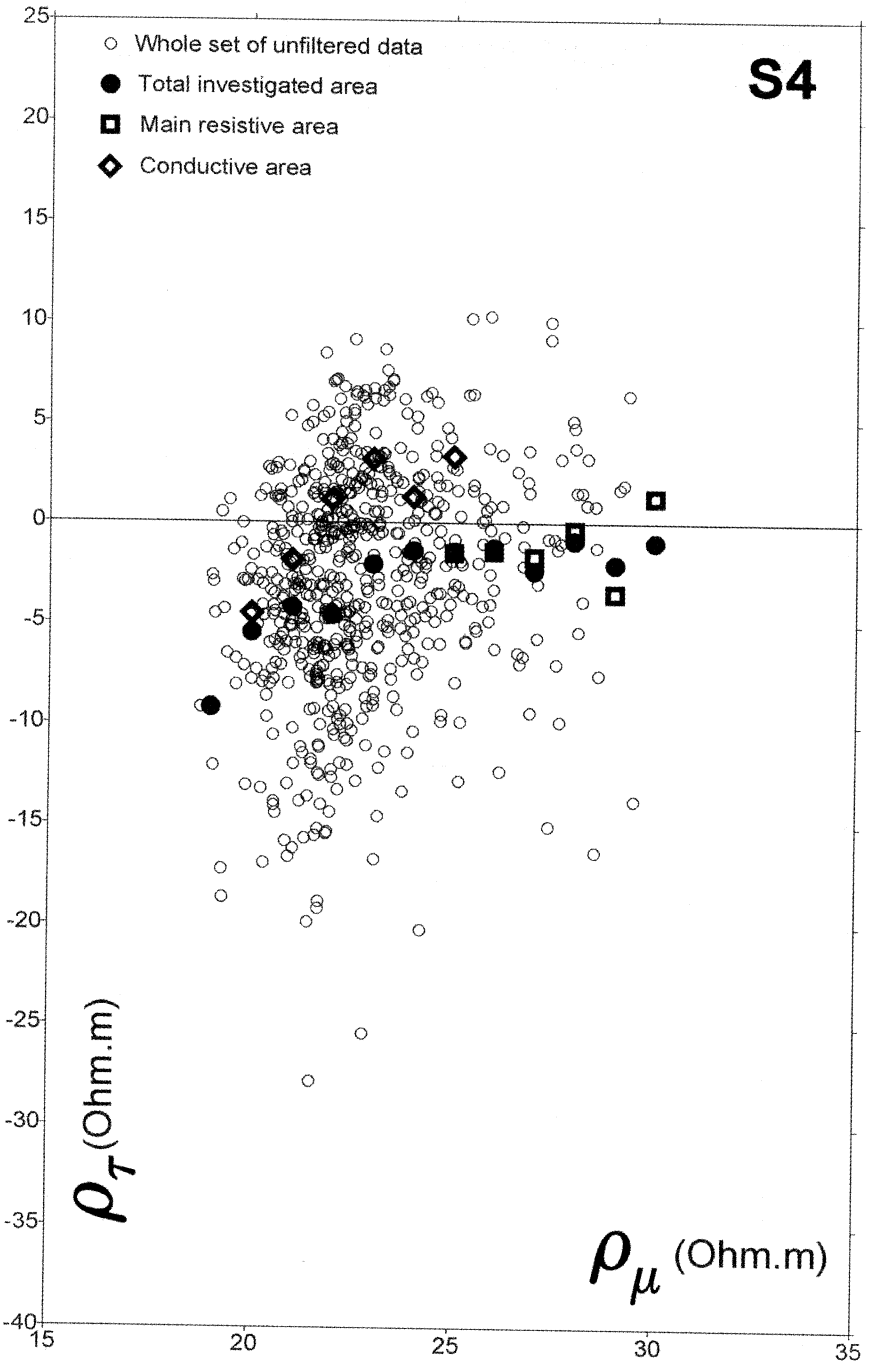

Fig. 10. Diagram of ρ_τ versus ρ_μ for S4 set of tripotential data. Filtered data (in bold) were obtained using moving average filtering with a box of 1 Ohm.m along the ρ_μ axis.

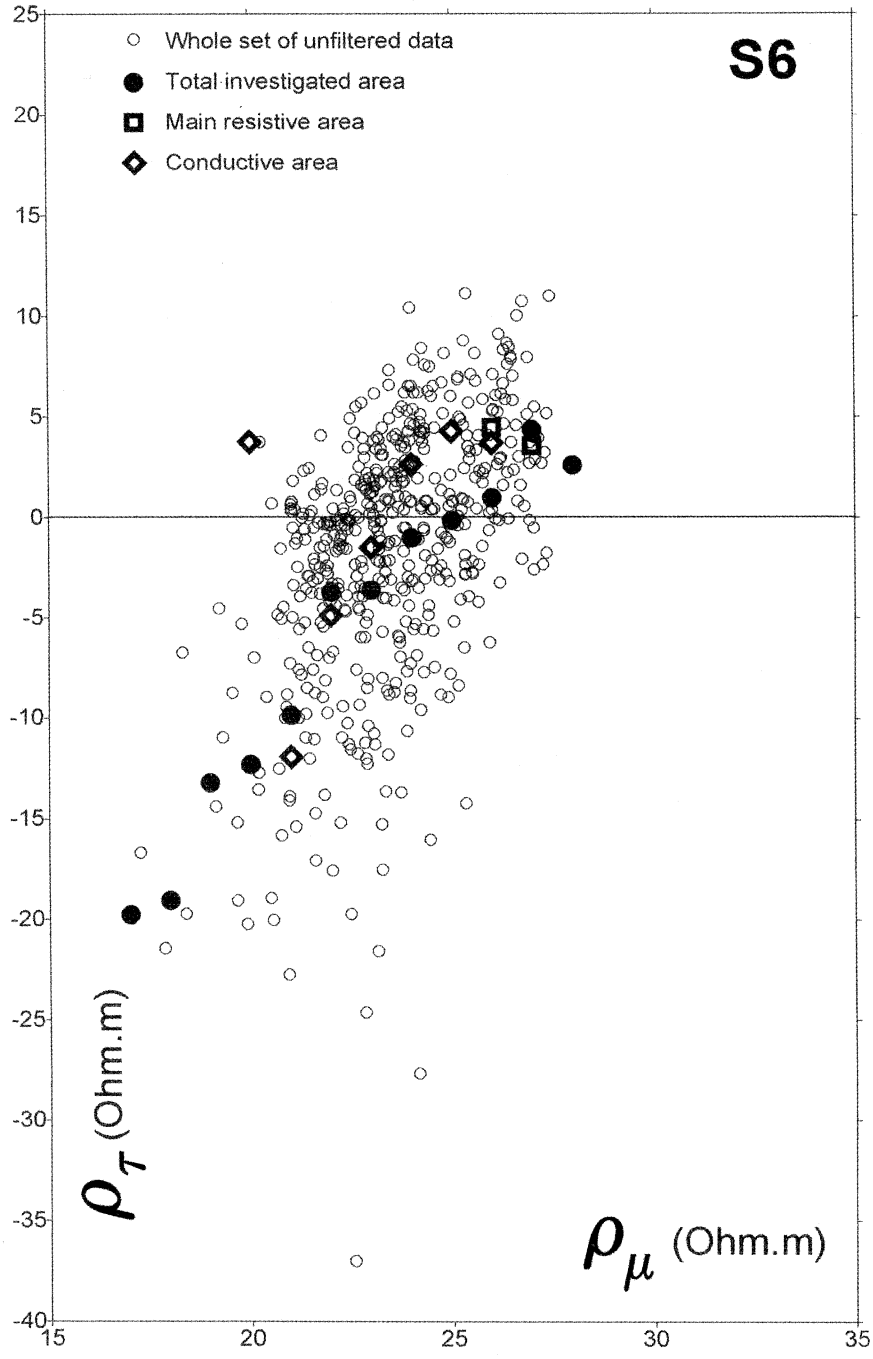

Fig. 11. Diagram of ρ_τ versus ρ_μ for S6 set of tripotential data. Filtered data (in bold) were obtained using moving average filtering with a box of 1 Ohm.m along the ρ_μ axis.

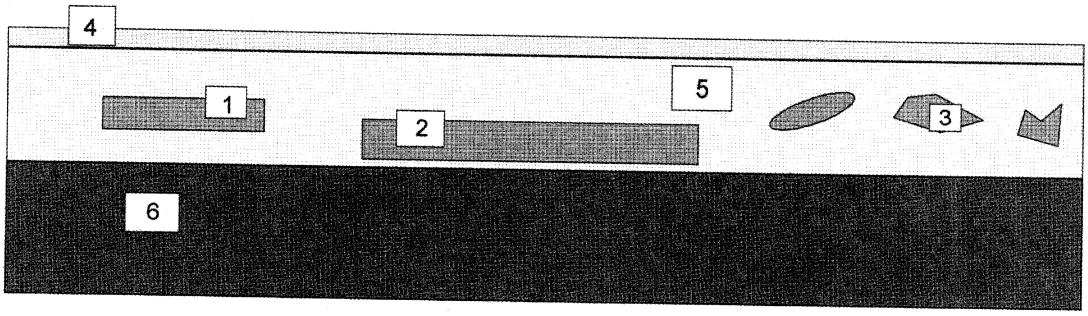

Fig. 12. A qualitative hypothetical rough model of three different places of the investigated area: 1 = main resistive (road); 2 = block basement; 3 = archaeological diffused bodies; 4 = weathered soil; 5 = alluvial clays; 6 = resistive bedrock.

5. Conclusions

The tripotential method integrated with dipole-dipole pseudosections, carried out with the system of data acquisition described above, seems to be expeditious, especially if it is computer-assisted during field survey and in data processing and interpretation.

This method seems to be very useful and reliable to solve archaeological problems which typically involve thin shallow layers, even though only an excavation campaign will ultimately test its reliability.

Finally it should also be stressed that the data comparison analysis in resistivity domain has the additional advantage of identifying some of the general and particular characteristics of the models both of the terrain and archaeological buried bodies.

Acknowledgements

The research described in this paper has been supported by a grant from Italian C.N.R., contribution No. 91.04219.ST75. We wish to thank the colleagues of the Institute of Archeology of the University of Palermo, namely Profs. N. Bonacasa, O. Belvedere and N. Allegro, for their help and useful suggestions.

REFERENCES

COLLETTI, G., P. COSENTINO, D. LUZIO and E. ROTIGLIANO (1995): The role of the contact resistance in the statistical distribution of the tripotential errors, in *Proceedings of the 1st Meeting of EEGS - European Section* (Turin, september 1995), 336-339.

COSENTINO, P. and D. LUZIO (1994): Tripotential data processing for H.E.S. interpretation, *Annali di Geofisica.*, **37** (suppl. 5), 1295-1302.

COSENTINO, P., E. GAGLIANO CANDELA and D. LUZIO (1992): Integrated geoelectrical investigations on the eastern hill of the Selinunte Archeological Park, *Boll. Geofis. Teor. Appl.*, **34**, 193-208.

COSENTINO, P., D. LUZIO and R. MARTORANA (1996): Inverse problem for tripotential measures in the study of buried cavities, *Annali di Geofisica*, **39**, 123-139 (this volume).

FRASER, D.C. (1981): Contour map presentation of dipole-dipole induced polarization data, *Geophys. Prospect.*, **29**, 639-651.

HABBERJAM, G.M. (1979): *Apparent Resistivity Observations and the Use of Square Array Techniques* (G. Borntraeger, Berlin), pp. 152.

HALLOF, P.G. (1957): On the interpretation of resistivity and induced polarization measurements, *Ph. D. Thesis* (Cambridge, MIT).